Electrochemical and Solid-State Letters, **14** (5) D45-D47 (2011)
1099-0062/2011/14(5)/D45/3/$28.00 © The Electrochemical Society

Modification of Porous Silicon Formation by Varying the End of Range of Ion Irradiation

Y. S. Ow,[z] H. D. Liang, S. Azimi, and M. B. H. Breese

Physics Department, National University of Singapore, 119260 Singapore

We have studied the influence of the end of range defects in silicon created by high energy protons and helium ions on subsequent porous silicon formation. The defect generation rate at the end of range is typically ten times higher than that close to the silicon surface. For low fluence irradiation, only the end-of-range region contains enough defects to prevent anodization whereas the low-defect regions closer to the surface are anodized. By varying the end-of-range depth over small lateral distances, silicon lines with tip radii of nanometers were fabricated for low fluence irradiation. For a high fluence irradiation we demonstrate how porous silicon formation is confined to buried channels by selectively producing regions on the silicon surface with two different ends of ranges.
© 2011 The Electrochemical Society. [DOI: 10.1149/1.3533438] All rights reserved.

Manuscript submitted November 22, 2010; revised manuscript received December 10, 2010. Published February 22, 2011.

A silicon micromachining process based on high-energy ion beam irradiation and electrochemical anodization to form porous silicon (PSi) has been used to fabricate patterned PSi and silicon microstructures, such as patterned distributed Bragg reflectors,[1] microturbines,[2] and concave silicon profiles.[3] Protons or helium ions, with energies of 250 keV to 2 MeV are focused to a beam spot of a few hundred nanometers for direct patterned irradiation on p-type silicon wafers. Irradiation causes localized increase in the resistivity arising from the point defects created along the ion trajectories.[4,5] Increased resistivity reduces the electrical hole current flowing through these regions during subsequent electrochemical anodization,[4] slowing down the PSi formation. PSi may then be easily removed with potassium hydroxide (KOH) to reveal underlying silicon microstructures. With high irradiation fluences, PSi formation ceases completely. A more recent development involves using standard ultraviolet photolithography to create patterned photoresist (PR) masks for shielding irradiation from a uniform broad ion beam.[3,6] This greatly improves irradiation in terms of irradiated area, time required and uniformity of fluence compared to using a focused ion beam. The experiments described here were performed using this method of irradiation. In addition, instead of simply stopping ions, PR with varying thicknesses were also used to selectively move the end-of-range region nearer to the silicon surface. The end-of-range region was then used to fabricate silicon lines with nanosized tips as well as buried PSi channels.

Experimental

The defect generation rate of high-energy ions in crystalline materials increases as the ions lose energy with increasing penetration depth.[7] Figure 1a show a stopping and range of ions in matter (SRIM) simulation[8] of the defects generated versus depth in silicon by 450 keV protons. The defect generation rate is as much as ten times higher at the end of range (~ 5.2 μm in silicon) compared to along their trajectories. Figures 1b–1c show how patterned PR with sloping sidewalls may be used to vary the end of range of protons laterally across a silicon wafer. As protons with well defined energies pass through a material, it comes to a gradual stop. In this case, the flat part of the PR is thick enough to completely stop the incoming protons from reaching the underlying silicon. However, protons are able to penetrate through the thinner sloping sidewalls of the PR to reach the silicon underneath. An example of a PR pattern (~ 6 μm thick) with sloping sidewalls is shown in Fig. 1d. The end-of-range defect profiles, both in the vertical and lateral sense, then follows that of the sloping PR sidewalls. After irradiation, the PR is removed and PSi is formed via electrochemical anodization. Regions of silicon shielded by the thick, flat PR are not irradiated and PSi forms normally while irradiated regions have a reduced PSi formation rate. The regions under the sloping sidewalls of the PR in particular, have the lowest PSi formation rate since the end of range is nearer to the surface and the defect generation at the end of range is much higher. Sloping silicon line structures following the sloping PR sidewall profiles are hence formed. With continued anodization, the initial exposed silicon line structures nearer to the surface continues inward to form PSi (orange region in Fig. 1c), resulting in tapering of the silicon line structures.

Figures 2a–2d show cross sectional scanning electron microscope (SEM) images of PSi multilayers which had 5 μm wide, 6 μm thick PR lines (AZ 4250) patterned on the surface and irradiated by a uniform broad 450 keV proton beam with different fluences. Multilayer PSi is formed simply by alternatively carrying out the electrochemical anodization with two different current densities, hence achieving PSi layers with alternating porosity.[6] A multilayer here serves the purpose of tracking the progression of the PSi formation. With a low fluence of $2 \times 10^{13}/\mathrm{cm}^2$ (Fig. 2a), the end-of-range defect density beneath the sloping part of the PR is not high enough to substantially slow PSi formation, hence no line structures are observed. This sample was then further anodized to have PSi form past the end of range. It is observed here that each PSi layer at the irradiated region is slightly thinner than that of the unirradiated region before the end of range. However, when anodization continues beyond this depth, the PSi layers formed are of the same thickness; an indication that hole current flowing through is now the same and that there are no irradiated defects at this depth.

The samples in Figs. 2b and 2c were fabricated in a similar fashion except that the fluences were higher and anodization was stopped just before the end-of-range. In Fig. 2b, the sample was irradiated with a fluence of $2 \times 10^{14}/\mathrm{cm}^2$, high enough for the silicon line structures to start forming (white dashed box). In Fig. 2c, an even higher fluence of $1 \times 10^{15}/\mathrm{cm}^2$ produces pronounced silicon lines with very fine tips. The inset of Fig. 2c shows that the tip radius is much smaller than 100 nm. It may also be seen here that the PSi formation over the irradiated regions is slower (hence thinner) than at the areas shielded by the PR. Figure 2e shows a sample prepared under identical conditions to Fig. 2c, after the removal of PSi. Figure 2d shows a sample which was irradiated with the highest fluence of $2 \times 10^{16}/\mathrm{cm}^2$. At this fluence, PSi formation ceases not only at the end of range, but all along the ion trajectory. Hence PSi has formed only at areas which were shielded by PR.

To further utilize our capability to modify the depth of the end-of-range defects with a PR and thus slow down or completely stop PSi formation, we patterned a multileveled PR pattern. After irradiation and anodization, buried PSi channels were formed. Figures 3a–3c show the schematics for forming these buried PSi channels. The multileveled PR was fabricated by first patterning 10 μm wide, 3 μm thick PR lines, and then patterning a second layer of PR lines with the same dimensions orthogonal to the first layer of PR lines. This way,

[z] E-mail: g0601170@nus.edu.sg

Downloaded 23 Feb 2011 to 137.132.250.14. Redistribution subject to ECS license or copyright; see http://www.ecsdl.org/terms_use.jsp

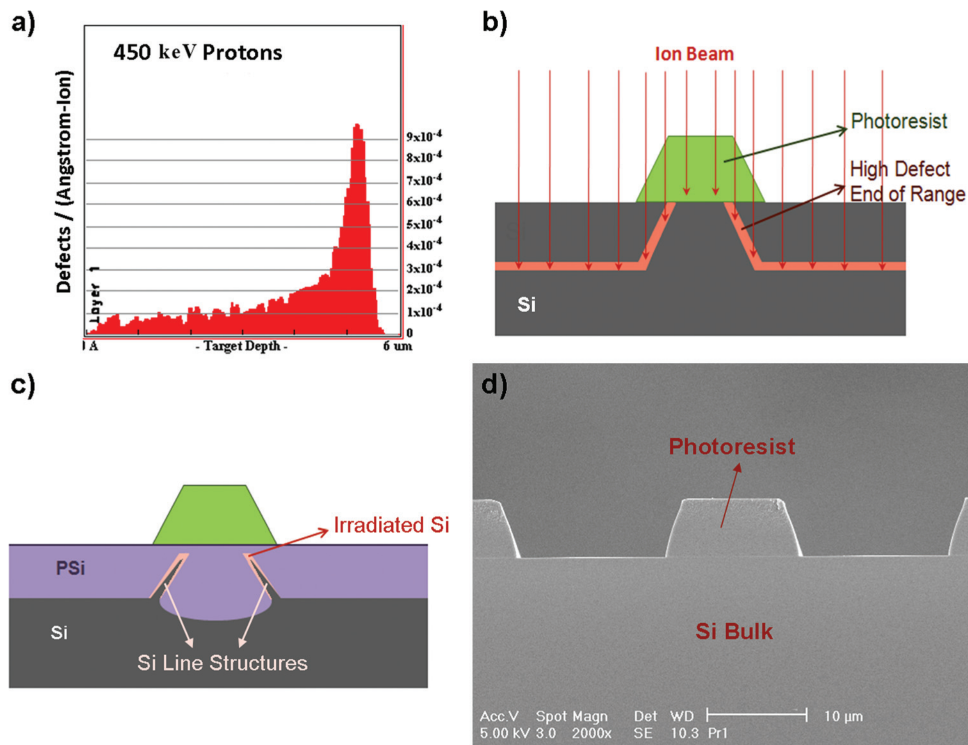

Figure 1. (Color online) (a) SRIM (Ref. 8) plot showing defects versus depth for 450 keV protons in silicon. (b), (c) schematics showing the fabrication of silicon lines with nanosized tips. (d) A cross sectional SEM image of a photoresist with sloping side-walls on silicon.

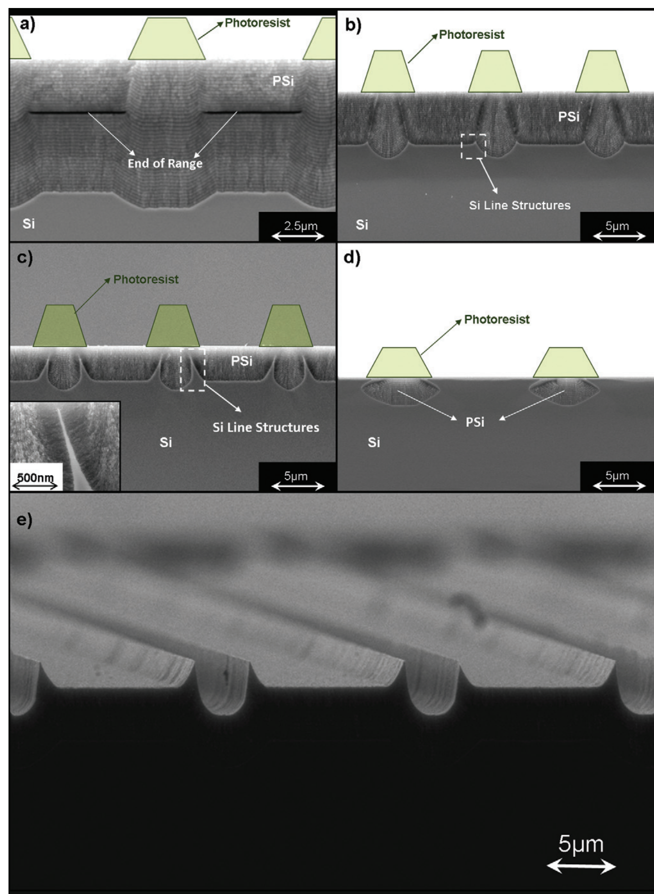

Figure 2. (Color online) (a)–(d) show cross sectional SEM images of multilayer PSi irradiated with fluences $2 \times 10^{13}/\text{cm}^2$, $2 \times 10^{14}/\text{cm}^2$, $1 \times 10^{15}/\text{cm}^2$, and $2 \times 10^{16}/\text{cm}^2$, respectively. Green trapezium indicates the locations of the PR during the irradiation. (e) Silicon line structures after the removal of PSi with KOH.

PR with different thicknesses on the same sample is achieved; double layered resists (6 μm thick), single layered resist (3 μm thick), as well as bare silicon surface. Irradiation was carried out with 1.5 MeV helium ions with a fluence of $1 \times 10^{15}/\text{cm}^2$. Helium ions are used here because being heavier than protons, the defect generation is higher ($\sim$20 times higher), resulting in a fluence high enough to completely stop PSi formation in a short irradiation time.

The end of range of 1.5 MeV helium ions is $\sim$5.2 μm in silicon, as shown in Fig. 4a. The thickest PR step is thick enough to stop the ions from reaching the silicon while the second PR step reduces their end of range in silicon, so the ions only penetrate the top $\sim$2 μm of the silicon surface. Regions of silicon which are not covered with PR are irradiated to a depth of $\sim$5.2 μm. During anodization, PSi formation starts at regions which were covered with the thickest PR. It continues by undercutting the regions underneath the second PR step and is confined at the sides as a result of the defects caused by the ions irradiating at parts of the silicon not covered with PR. The result is a buried PSi channel under the second PR step. This can be seen from the plan view SEM image in Fig. 4b. Regions from the surface where PSi starts to form and the buried PSi channels are indicated. However, as PSi formation is not confined from the bottom since it was not irradiated, further anodization would allow PSi formation to proceed deeper into the bulk and at the same time, undercut all irradiated regions as can be seen in Figs. 4c and 4d. By simply obtaining suitable PR patterns and selecting the correct energy and ions to use, we may create buried PSi channels of different dimensions as long as care is taken not to over anodize for PSi to form past the end of range of the ions.

Conclusion

We have studied the effects of ions' end-of-range defects on PSi formation. This was compared to the defects generated along trajectories is different primarily in the defects generation rate. This allows us to locally modify wafer resistivity in the lateral and vertical directions in conjunction with variable thickness PR, enabling us to fabricate silicon lines with nanosized tips. These silicon line structures may find applications in nanoimprinting lithography[9,10] while the grooves between every two silicon line structures may be

Downloaded 23 Feb 2011 to 137.132.250.14. Redistribution subject to ECS license or copyright; see http://www.ecsdl.org/terms_use.jsp

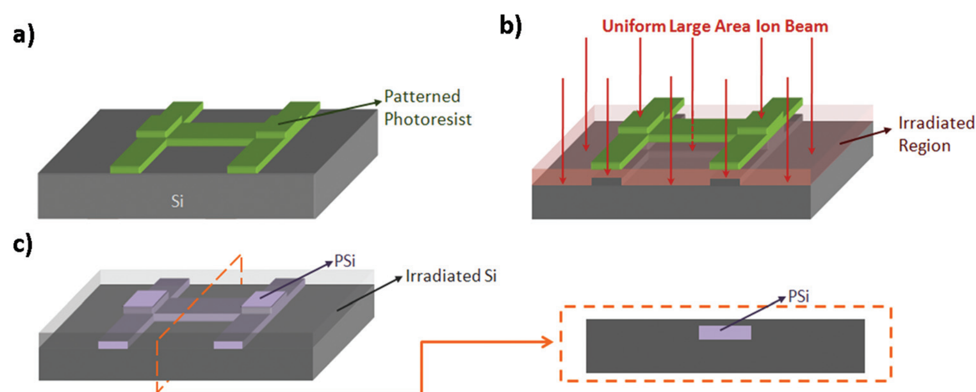

Figure 3. (Color online) (a), (b) schematics showing the processes involved to achieve buried PSi channels formation.

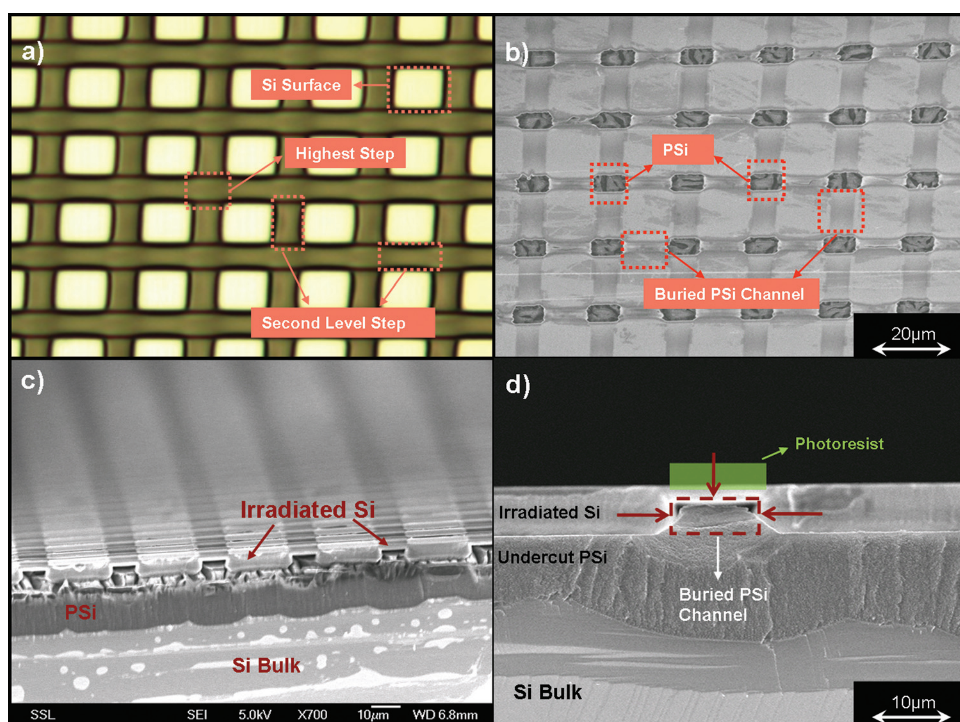

Figure 4. (Color online) (a) Optical image of multileveled PR patterned on silicon. Thickest PR step is where two PR lines overlap. (b) Shows a planar SEM image of the sample. (c) A cross sectional SEM image of the irradiated and anodized sample. (d) A magnified cross sectional SEM image of the irradiated and anodized sample. Red arrows indicate the planes where PSi formation is confined. Samples in (c) and (d) were intentionally over anodized to demonstrate PSi undercutting all irradiated regions.

used as channels for microfluidics devices.[11] Also, by utilizing multilevel PR masks, we are able to achieve confined PSi formation to fabricate buried PSi channels as well as undercut silicon structures. With the removal of the PSi with KOH, these buried channels may be used as buried contacts for silicon solar cells,[12] silicon microchannel heat sink,[13] or even channels for microfluidic devices.[14]

Acknowledgment

The authors acknowledge the financial support from the MOE Academic Research Fund under grant no. R144 000 238 112.

National University of Singapore assisted in meeting the publication costs of this article.

References

1. D. Mangaiyarkarasi, M. B. H. Breese, Y. S. Ow, and C. Vijila, *Appl. Phys. Lett.*, **89**, 021910 (2006).
2. I. Rajta, S. Z. Szilasi, P. Furjes, Z. Fekete, and C. Ducso, *Nucl. Instrum. Methods Phys. Res. B*, **267**, 2292 (2009).
3. Y. S. Ow, M. B. H. Breese, and S. Azimi, *Opt. Express*, **18**, 14511 (2010).
4. M. B. H. Breese, F. J. T. Champeaux, E. J. Teo, A. A. Bettiol, and D. J. Blackwood, *Phys. Rev. B*, **73**, 035428 (2006).
5. V. Lehmann, *Electrochemistry of Silicon: Instrumentation, Science, Materials and Applications*, Wiley-VCH, New York (2002).
6. D. Mangaiyarkarasi, O. Y. Sheng, M. B. H. Breese, V. L. S. Fuh, and E. T. Xioasong, *Opt. Express*, **16**, 12757 (2008).
7. A. Brown and H. Suit, *Radiother. Oncol.*, **73**, 265 (2004).
8. J. F. Ziegler, M. D. Ziegler, and J. P. Biersack, *Nucl. Instrum. Methods Phys. Res. B*, **268**, 1818 (2010).
9. Y. Zhao, E. Berenschot, H. Jansen, N. Tas, J. Huskens, and M. Elwenspoek, *Microelectron. Eng.*, **86**, 832 (2009).
10. P. B. Grabiec, M. Zaborowski, K. Domanski, T. Gotszalk, and I. W. Rangelow, *Microelectron. Eng.*, **73–74**, 599 (2004).
11. V. Fekete, D. Clicq, W. De Malsche, H. Gardeniers, and G. Desmet, *J. Chromatogr. A*, **1130**, 151 (2006).
12. P. Vitanov, E. Goranova, V. Stavrov, P. Ivanov, and P. K. Singh, *Sol. Energy Mater. Sol. Cells*, **93**, 297 (2009).
13. D. Bogojevic, K. Sefiane, A. J. Walton, H. Lin, and G. Cummins, *Int. J. Heat Fluid Flow*, **30**, 854 (2009).
14. D.-S. Kim, J.-E. Park, J.-K. Shin, P. K. Kim, G. Lim, and S. Shoji, *Sens. Actuators B*, **117**, 488 (2006).

Downloaded 23 Feb 2011 to 137.132.250.14. Redistribution subject to ECS license or copyright; see http://www.ecsdl.org/terms_use.jsp